PROCEEDINGS OF SPIE

SPIEDigitalLibrary.org/conference-proceedings-of-spie

Coating of thin, lightweight x-ray mirrors without distortion

Peter Solly, William Zhang, David Windt, Youwei Yao

Peter M. Solly, William Zhang, David Windt, Youwei Yao, "Coating of thin, lightweight x-ray mirrors without distortion," Proc. SPIE 12181, Space Telescopes and Instrumentation 2022: Ultraviolet to Gamma Ray, 121814P (31 August 2022); doi: 10.1117/12.2629540

SPIE.

Event: SPIE Astronomical Telescopes + Instrumentation, 2022, Montréal, Québec, Canada

Downloaded From: https://www.spiedigitallibrary.org/conference-proceedings-of-spie on 01 Sep 2022 Terms of Use: https://www.spiedigitallibrary.org/terms-of-use

Coating of Thin, Lightweight X-ray Mirrors Without Distortion

Peter M. Solly*[a,b], William W. Zhang[b], David Windt[c], Youwei Yao[d]

[a]KBR Space Engineering Division, 7701 Greenbelt Road, Suite 400, Greenbelt, Maryland 20770, USA
[b]NASA Goddard Space Flight Center (GSFC), Greenbelt, MD USA 20771, USA
[c]Reflective X-ray Optics LLC, 1361 Amsterdam Ave, Suite 3B, New York, NY 10027, USA
[d]MIT Kavli Institute for Astrophysics and Space Research, Space Nanotechnology Laboratory, Cambridge, Massachusetts, USA

ABSTRACT

The manufacturing of lightweight silicon X-ray mirrors requires the application of a low stress thin film coating to the optical reflecting surface to achieve high performance. Coating of high-density materials such as iridium, is necessary to increase reflectivity at high energies above 4 keV, but presents many challenges, primarily the large distortions to the thin silicon substrates that occur from these highly stressed layers. The ideal solution to this problem is to perfectly balance the thin film stress on the front reflective surface with an equal layer on the backside of the mirror.

Two approaches will be discussed in this paper. First is magnetron sputtering of thin film iridium using Ion Beam Figuring (IBF) of a thick silicon oxide layer on the back surface derived algorithmically from optical metrology data to compensate the residual stresses from the imperfections of the sputter coating process. Second is the application of thin coating using Atomic Layer Deposition (ALD), a process that is uniform at the atomic layer. Results of experiments from both processes will be presented, showing that either process is suitable for future X-ray telescopes, with the ALD process being preferable for its consistent higher performance and simplicity.

Keywords: silicon mirrors, X-ray optics, optimization, finite element model, thin film coating, Iridium, IBF, ALD

*Peter M Solly, peter.m.solly@nasa.gov

1. INTRODUCTION

Future proposed X-ray telescopes, from sounding rocket missions such as OGRE [1] and MIDEX missions such as STAR-X [2] to flagship missions such as Lynx [3], will rely on thin segmented optics such as the polished silicon optics being developed at GSFC [4]. These segments will be mass produced using highly refined fabrication techniques [5], with quantities possibly in the tens of thousands. These individual segments will then be aligned and bonded [6] into large mirror assemblies, such as the one seen in Figure 1-1.

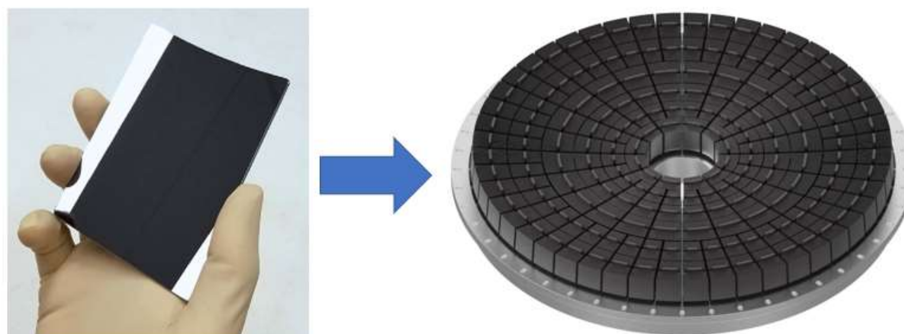

Figure 1-1 Polished Silicon Mirrors from Individual Segment to Mirror Assembly

Space Telescopes and Instrumentation 2022: Ultraviolet to Gamma Ray, edited by Jan-Willem A. den Herder, Shouleh Nikzad, Kazuhiro Nakazawa, Proc. of SPIE Vol. 12181, 121814P · © 2022 SPIE · 0277-786X · doi: 10.1117/12.2629540

Downloaded From: https://www.spiedigitallibrary.org/conference-proceedings-of-spie on 01 Sep 2022
Terms of Use: https://www.spiedigitallibrary.org/terms-of-use

As a final step in the segment fabrication process, each mirror must be coated with a high-density material to enhance the optics X-ray reflectivity at energies above 4 keV. These materials are inherently high stress, and when that stress is combined with the high aspect ratio of polished silicon mirrors (approximately 100mm in length/width while just 0.5mm thick) it can impart significant distortion on the mirrors figure. If the mirror is coated on the front surface and the back surface, the variations in thickness and uniformity of the coating must be extremely small for the applied stresses to balance each other and leave the mirror un-deformed. The coating process must also be amenable to mass production, both in complexity and time, to meet the schedule and cost requirements of such a large assembly.

2. METHODS

Two methods have recently been shown to meet the exacting standards required for high resolution X-ray telescopes using polished silicon optics: iterative stress balancing using silicon oxide compensation and ALD.

2.1 Silicon Oxide Stress Compensation

The first method for high energy coatings is using the inherent stress of thermally grown silicon oxide on the back of the mirror to balance out the residual stresses from magnetron sputtered coatings. A correction profiles is determined by using a mathematical algorithm derived from mirror interferometer measurements, and then applied via Ion Beam Figuring (IBF) of the back surface oxide.

2.1.1 Mathematical Description of Compensation Algorithm

The process makes use of the following mirror surface figure measurements:

- M0: Initial mirror, polished and IBF to high quality
- M1: Oxide grown on both sides
- M2: Front Oxide stripped
- M3: Iridium coated
- M4: Iridium annealed

Each mirror measurement consists of a list of y data points representing each pixel:

$$M_i = \left\langle \begin{matrix} \theta_1 \\ \vdots \\ \theta_y \end{matrix} \middle| \begin{matrix} z_1 \\ \vdots \\ z_y \end{matrix} \middle| \begin{matrix} h_1 \\ \vdots \\ h_y \end{matrix} \right\rangle \quad (1)$$

Where θ and z are unit vectors from -1 to 1. For each measurement, we calculate a two-dimensional Chebyshev polynomial fit of the surface. This decomposes the surface (ρ) measurement into a summation:

$$\rho(\theta, z) = \sum_{i,j=0}^{N} A_{i,j} * T_i(\theta) * T_j(z) \quad (2)$$

Where i and j represent the order in the azimuthal and axial directions, respectively, and T represent the Chebyshev polynomials:

$$T_0(x) = 1, \;\; T_1(x) = x, \;\; T_2(x) = 2x^2 - 1, \;\; T_3(x) = 4x^3 - 3x, \;\; \ldots \quad (3)$$

If the mirror image is decomposed into N orders along each axis, the resulting coefficients form a square matrix, A, of size (N+1) x (N+1):

$$A = \begin{bmatrix} A_{0,0} & \cdots & A_{0,N} \\ \vdots & \ddots & \vdots \\ A_{N,0} & \cdots & A_{N,N} \end{bmatrix} \quad (4)$$

To perform this decomposition, we must calculate a 2-D pseudo-Vandermonde matrix of the θ and z values:

Downloaded From: https://www.spiedigitallibrary.org/conference-proceedings-of-spie on 01 Sep 2022
Terms of Use: https://www.spiedigitallibrary.org/terms-of-use

$$V[\dots,(N+1)*i+j]=T_i(\theta)*T_j(z) \quad (5)$$

Which then satisfies the equation:

$$VA^*=[h] \quad (6)$$

Where [h] is the list of measured image heights from M, and A* is the flattened (row order) A matrix such that:

$$A^*=[A_{0,0,}\dots A_{0,N},A_{1,0}\dots A_{N,N}] \quad (7)$$

This equation can be solved for A by calculating the (Moore-Penrose) pseudo-inverse matrix of V. After the image decomposition has been performed, we must set the first two columns of the A matrices to 0, as these represent radius and tip/tilt errors that cannot be accurately measured by the interferometer.

A finite element model is then generated to develop a stress profile to match the mirror measurements. Unit stress profiles, U, are generated as two dimensional Chebyshev polynomials, similar to equation 3, and applied to the back surface of the mirror. If the stress profiles are generated for K orders along each axis, there will be (K+1)2 total profiles generated. For each profile, the resulting mirror surface deformation from the FE model is calculated, and a fitting process identical to equation 4 can be performed. Theses profile vectors are then flattened and combined as the columns of a coefficient matrix:

$$C=\begin{bmatrix} C_{0,0} & \cdots & C_{0,K^*} \\ \vdots & \ddots & \vdots \\ C_{N^*,0} & \cdots & C_{N^*,K^*} \end{bmatrix} \quad (8)$$

Where:

$$N^*=(N+1)^2 \quad (9)$$

$$K^*=(K+1)^2 \quad (10)$$

To determine the stress caused by oxide/coating, we must first calculate the difference in mirror surface images:

$$D_{oxide}=A_2-A_0 \quad (11)$$

$$D_{coating}=A_4-A_2 \quad (12)$$

Each image change can be correlated to FE results using the following equation:

$$Cb=D^* \quad (13)$$

Which can be solved for b by again using the pseudo-inverse matrix of C. The scalar coefficients, b, can then be applied to the unit profiles to generate stress profiles:

$$S=\sum_{0}^{K^*} b_i*U_i \quad (14)$$

The correction map can then be determined using the stress profiles of both the oxide and coating:

$$S_d=S_{oxide}-S_{coating} \quad (15)$$

We then scale the stress difference, S_d, by the oxide thickness used in the FEM unit cases to determine the input values to IBF correction.

Downloaded From: https://www.spiedigitallibrary.org/conference-proceedings-of-spie on 01 Sep 2022
Terms of Use: https://www.spiedigitallibrary.org/terms-of-use

2.1.2 Oxide Thickness

Using uniform IBF removal, the oxide layer on the front surface of the mirror is removed. This process can be done iteratively with smaller quantities to confirm the thickness of the oxide layer. The measured figure change, primarily in sag coefficients, can then be combined with FEM analysis to determine various parameters of the oxide. For the mirror 312P1025, measurements before and after 100nm of uniform removal, combined with known material properties and Hooke's law, yield an estimated stress from the oxide layer of 303 MPa. The front surface oxide thickness can be determined by the sag changes in the removal runs, in this case the thickness was found to be 182 nm. Using this thickness on the front as well as the sides, and the small difference in sag measured in M0 and M1 mirror measurements, combined with the FEM values previously determined, shows higher oxide growth on the back of the mirror, estimated to be 193 nm. Higher growth on the convex surface is expected from previous experiments [7]. A FEM can be generated with these estimated stresses/thicknesses and is compared to the oxide removed measurement (M2), shown in Figure 2-1 as a very good match.

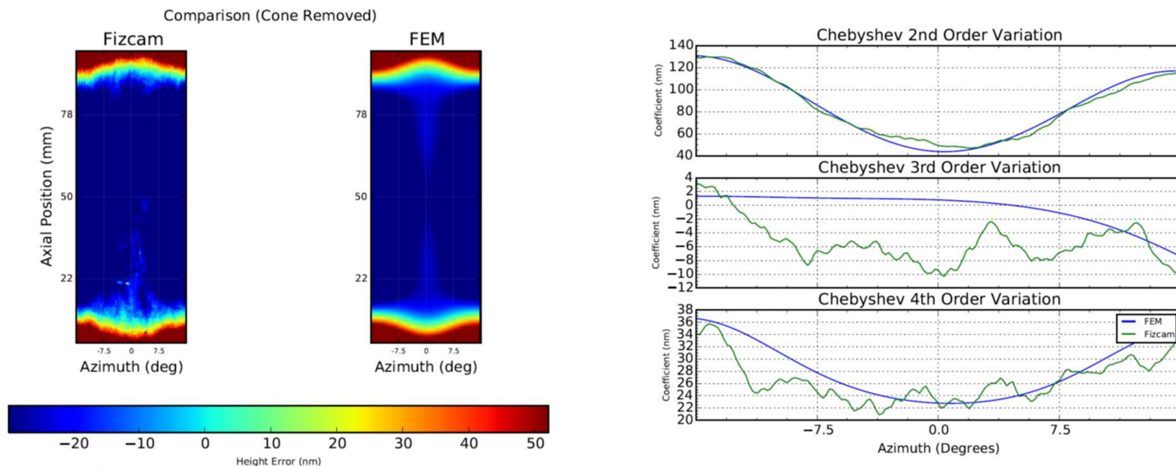

Figure 2-1 Comparison of FE Model to Measured Mirror with Back Surface Silicon Oxide

2.1.3 Iridium Coating

Two mirrors (312P1025 and 312S1050) were coated with 5 nm chromium and 30 nm of iridium. The chromium layer acts as a binding agent for the mirror surface. The stress generated by Iridium coating is approximately 3500 MPa, a factor of ~12x higher than silicon dioxide. The mirror deformation is related to both applied stress and thickness of the thin film, so the main metric to examine is integrated stress, which is the coating stress multiplied by the thickness. The 30 nm of Iridium has an expected integrated stress of 105 N/m. The calculated integrated stress profiles of these two mirrors, using the method detailed in the previous section, are shown below in Figure 2-2.

Downloaded From: https://www.spiedigitallibrary.org/conference-proceedings-of-spie on 01 Sep 2022
Terms of Use: https://www.spiedigitallibrary.org/terms-of-use

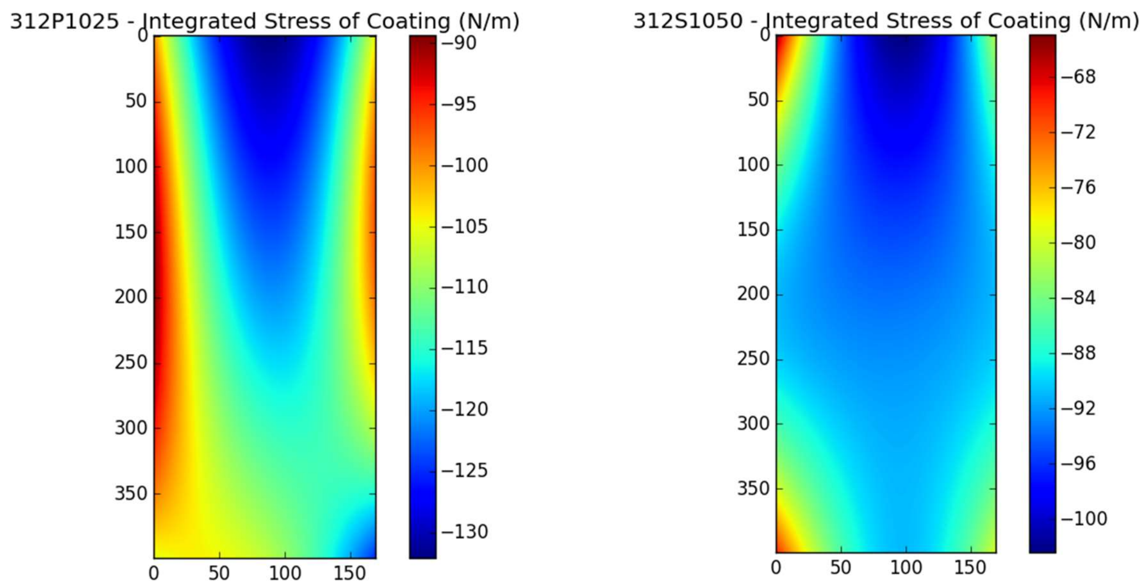

Figure 2-2 Integrated Stress of 30nm Iridium Coating Using Magnetron Sputter

The stress map of the surface shows an average integrated stress of 111.8 N/m for 321P1025 and 102.0 N/m for 312S10150, compared the expected value of 105 N/m. The stress values indicate average iridium thicknesses of 31.9 nm and 29.1 nm respectively. The variation across an individual mirror would be +/- 6nm, which is more likely a result of systematic error from attempting to translate the FEM profiles to the interferometer measurements. These errors can be disregarded when attempting to equate the iridium stress with the oxide stress, which is calculated with the same method and would exhibit the same systematic error. Integrated stresses from the back surface oxide layers are shown in Figure 2-3, where the average integrated stress from oxide for the two mirrors was 67.1 N/m and N/m MPa, respectively.

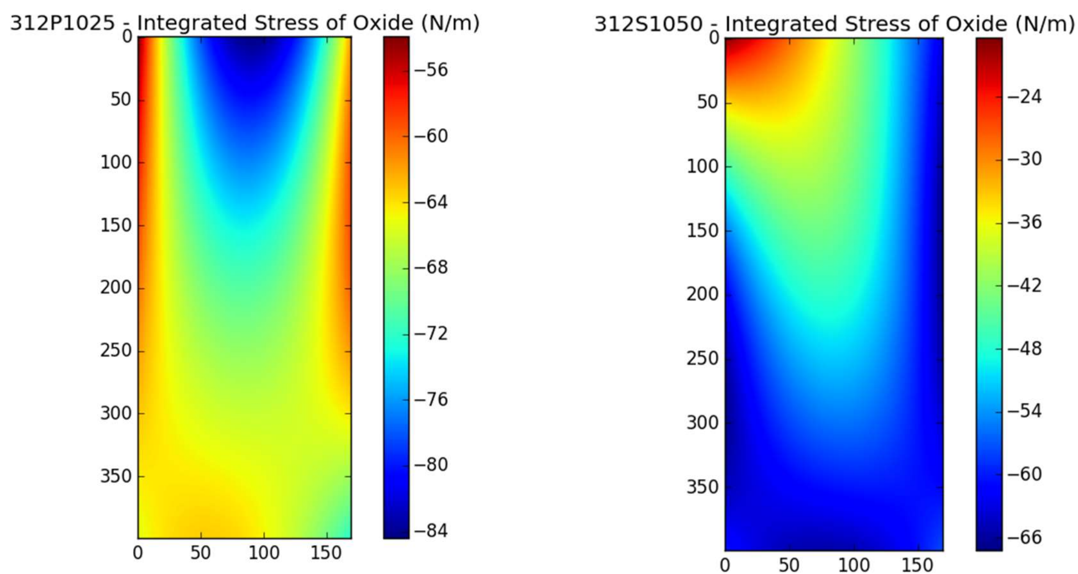

Figure 2-3 Integrated Stress of ~190nm Thermally Grown SiO_2 on Back Surface

Downloaded From: https://www.spiedigitallibrary.org/conference-proceedings-of-spie on 01 Sep 2022
Terms of Use: https://www.spiedigitallibrary.org/terms-of-use

2.1.4 Annealing

It's clear from the previous section results that the iridium stress is much higher than the oxide stress, by nearly a factor of 2. To use oxide to correct the mirror, the iridium stress must be lower than the oxide. To accomplish this, and to improve the stability of the coating (to any future heat loadings such as heat curing epoxy), the mirrors are annealed. These two mirrors were annealed at 300 °C for two hours with two-hour ramp up/ramp down. After annealing, average integrated stress in 312P1025 was 43.1 N/m, while 312S1050 was 39.9 N/M. These values represent a residual stress of 39% of the original coating stress. This annealing reduction is in line with previously published data [8]. Iridium begins to crystallize above 350 °C [9][10], so annealing temperature should be limited to 300 °C.

2.2 Atomic Layer Deposition

The Atomic Layer Deposition (ALD) process is an established technique. The ALD recipe consists of alternating pulses of various pre-cursor elements. These elements bond to each other in single layers, producing alternating but atomically uniform layers, as shown in Figure 2-4.

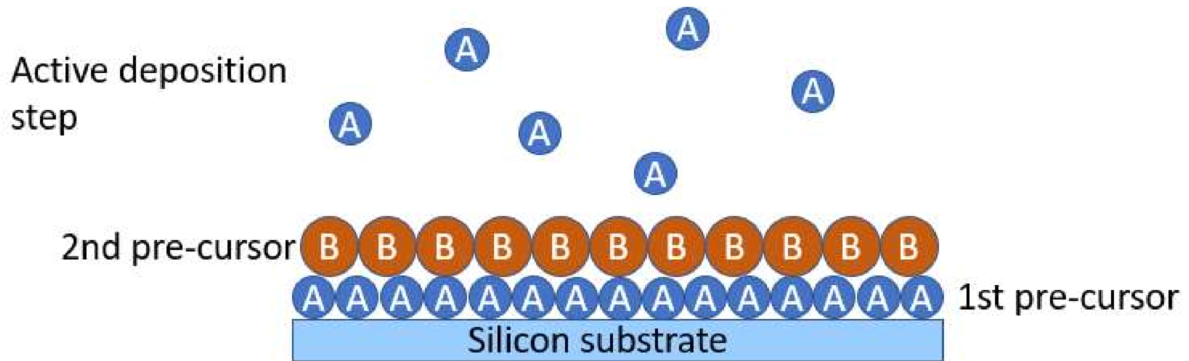

Figure 2-4 Schematic of Atomic Layer Deposition Process

This surface uniformity results in a surface stress with nearly zero variation. When both sides of the mirror are coated, the uniform stresses balance each other, and the mirror therefore does not suffer any deformation.

3. RESULTS

Experiments have been carried out demonstrating the viability of both coating methods. Two mirrors were subjected to the silicon oxide stress compensation method, with a final coating of 30 nm of Iridium. Four mirrors were coated using ALD, two with a combination of platinum/aluminum oxide and two with 20 nm of platinum. Each method showed a final mirror that would meet the most stringent mission requirements.

3.1 Silicon Oxide Stress Compensation

Two silicon mirrors, 312P1025 and 312S1050, were used in the first experiment using oxide stress compensation. The full sequence of measurements and steps is detailed in the previous section. A slower and more detailed approach was taken with 312P1025, where the FE models were carefully tuned, and the final IBF removal on the back surface was split into two separate runs, so that the final correction could be fine-tuned using the correlated result of the first correction run. For 312S1050 a more streamlined approach was attempted without individualized model correlation and a single corrective pass, to better understand the impacts of the mass production approach that would be required

Downloaded From: https://www.spiedigitallibrary.org/conference-proceedings-of-spie on 01 Sep 2022
Terms of Use: https://www.spiedigitallibrary.org/terms-of-use

for a large mission. A summary of the measured sag, as well as the surface RMS (radius, cone, and sag removed) for each step of the process for 312P1025 is shown in Table 3-1.

Table 3-1 Backside Oxide Stress Compensation Distortion Summary for 312P1025 By Process Step

312P1025 Measurements	RMS (nm)	Sag (nm)	
		Mean	P-V
Polished	4.1	84.3	14.4
Oxide Growth	20.9	176.3	93.4
Coated (30nm IR)	13.9	21.5	46.7
Annealed (300 °C)	9	118.5	53.5
Backside IBF 1st Iteration	6.9	101.5	36.1
Backside IBF Final Iteration	6.5	82.8	16.0

A comparison of the un-coated mirrors and the final coated/compensated mirrors can be found in Figure 3-1 and Figure 3-2. A comparison of the relevant image metrics is summarized in Table 3-2.

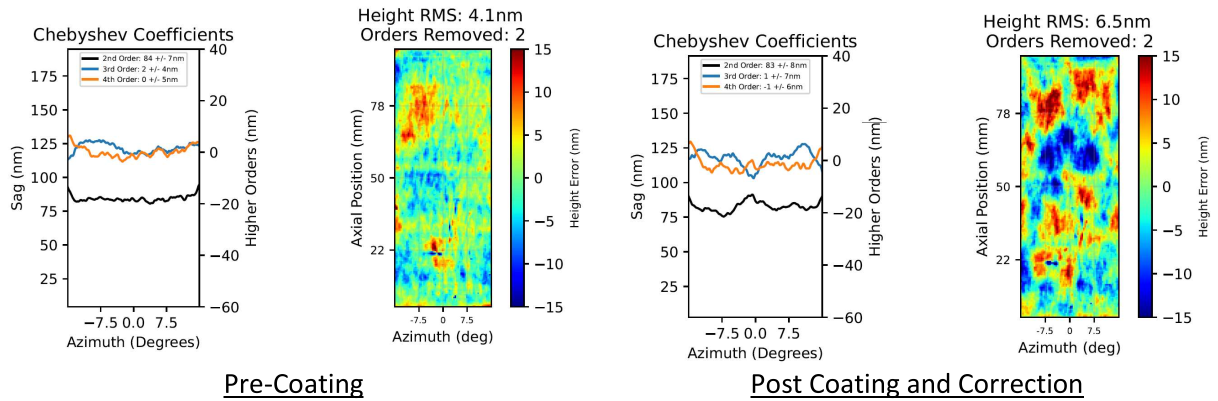

Figure 3-1 Backside Compensation Mirror Figure Comparison for 312P1025

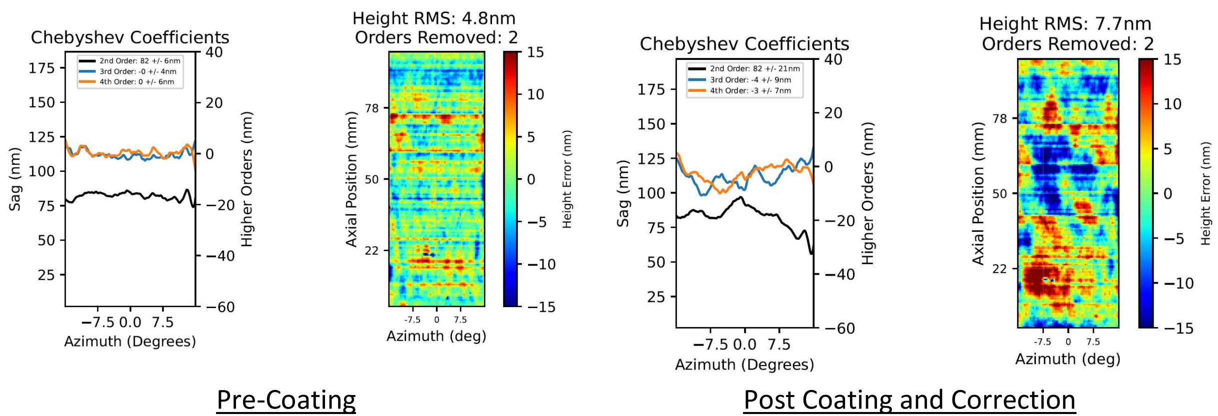

Figure 3-2 Backside Compensation Mirror Figure Comparison for 312S1050

Table 3-2 Backside Compensation Mirror Figure Change Summary

Mirror	Coating	Pre-Coat Surface Values (nm)			Post-Coat Surface Values (nm)			Net Change (nm)		
		Sag (Mean)	Sag (PV)	RMS	Sag (Mean)	Sag (PV)	RMS	Sag (Mean)	Sag (PV)	RMS
312P1025	30nm Ir	84.3	14.4	4.1	82.8	16.0	6.5	-1.5	1.6	2.4
312S1050	30nm Ir	81.9	12.6	4.8	82.4	41.0	7.7	0.5	28.4	2.9

Downloaded From: https://www.spiedigitallibrary.org/conference-proceedings-of-spie on 01 Sep 2022
Terms of Use: https://www.spiedigitallibrary.org/terms-of-use

The image degradation during coating is dominated by sag change, particular sag variation across the azimuth. This is highlighted in the second mirror, 312S1050, which attempted a full correction in a single backside IBF pass. The lack of an initial calibration run led to a significant amount of sag variation remaining in the mirror. The first mirror, 312P1025, shows that when the removal is calibrated specifically to the individual mirror, this sag variation can be corrected. A comparison of the final image to a prediction generated by the compensation algorithm shows a very good match for 312P1025, indicating the stress from the oxide is behaving as expected when well calibrated, shown in the full sequence of images in Figure 3-3.

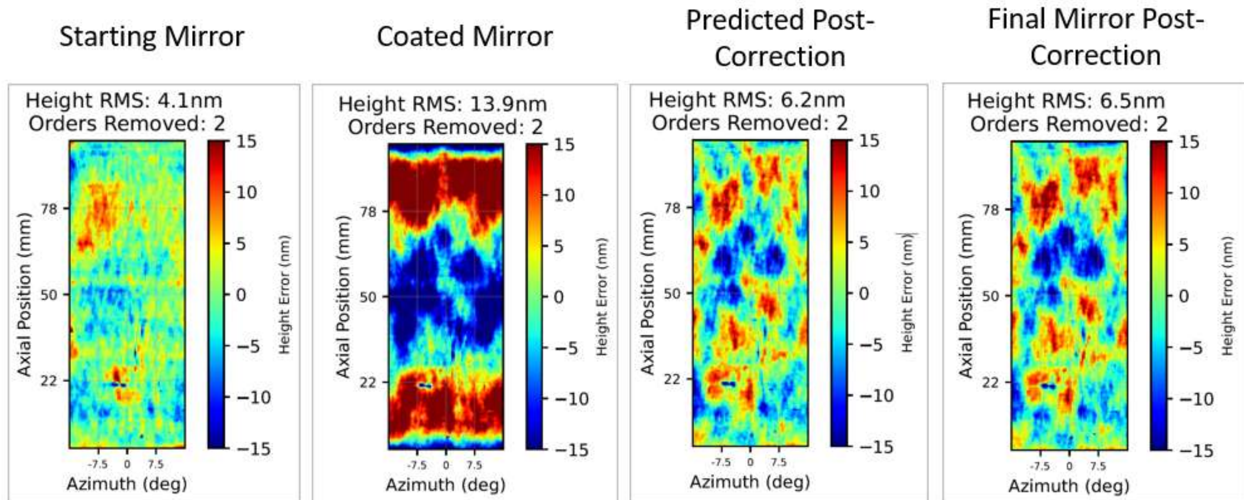

Figure 3-3 Image Comparison of 312P1025 With Final Predicted Distortion

As a final confirmation, the mirror is measured using X-ray reflectometry. The measurements in Figure 3-4 show good surface roughness, with measured Iridium thicknesses of 28.4nm for 312P1025 and 28.6nm for 312S1050.

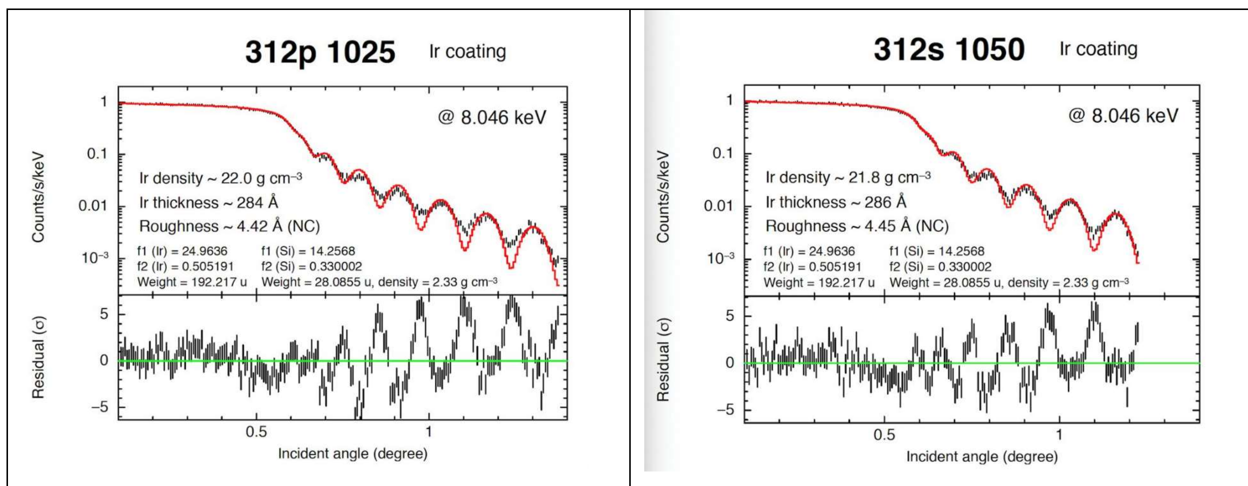

Figure 3-4 X-ray Reflectometry Measurements of Backside Compensation Mirror

Downloaded From: https://www.spiedigitallibrary.org/conference-proceedings-of-spie on 01 Sep 2022
Terms of Use: https://www.spiedigitallibrary.org/terms-of-use

3.2 Atomic Layer Deposition

Four silicon mirrors were coated using the ALD method. A summary of the main distortion measurements is shown in Table 3-3.

Table 3-3 ALD Coating Mirror Figure Change Summary

Mirror	Coating	Pre-ALD Surface Values (nm)			Post-ALD Surface Values (nm)			Net Change (nm)		
		Sag (Mean)	Sag (PV)	RMS	Sag (Mean)	Sag (PV)	RMS	Sag (Mean)	Sag (PV)	RMS
330P1081	20nm Pt	508.6	14.3	4.2	509.3	16.8	4.9	0.7	2.5	0.7
330P1077	20nm Pt	510.4	11.0	3.8	513.9	11.6	4.0	3.5	0.6	0.2
311P2000	8nm Pt + 7nm Al_2O_3	95.6	15.8	4.2	101.5	17.2	3.9	5.9	1.4	-0.3
335S1080	8nm Pt + 7nm Al_2O_3	544.8	14.7	3.6	542.1	14.6	4.4	-2.7	-0.1	0.8

It is clear from these measurements that the ALD process worked as anticipated, leaving nearly no un-balanced stress in the mirror. No significant changes in figure were measured, the small changes measured are within the normal metrology noise for the interferometer. Images of a platinum coated mirror can be seen in Figure 3-5.

Figure 3-5 Images of Mirror Coated With 20nm Platinum Using ALD

Downloaded From: https://www.spiedigitallibrary.org/conference-proceedings-of-spie on 01 Sep 2022
Terms of Use: https://www.spiedigitallibrary.org/terms-of-use

Detailed image comparisons of the pre and post ALD interferometer measurements can be seen in Figure 3-6 thru Figure 3-9.

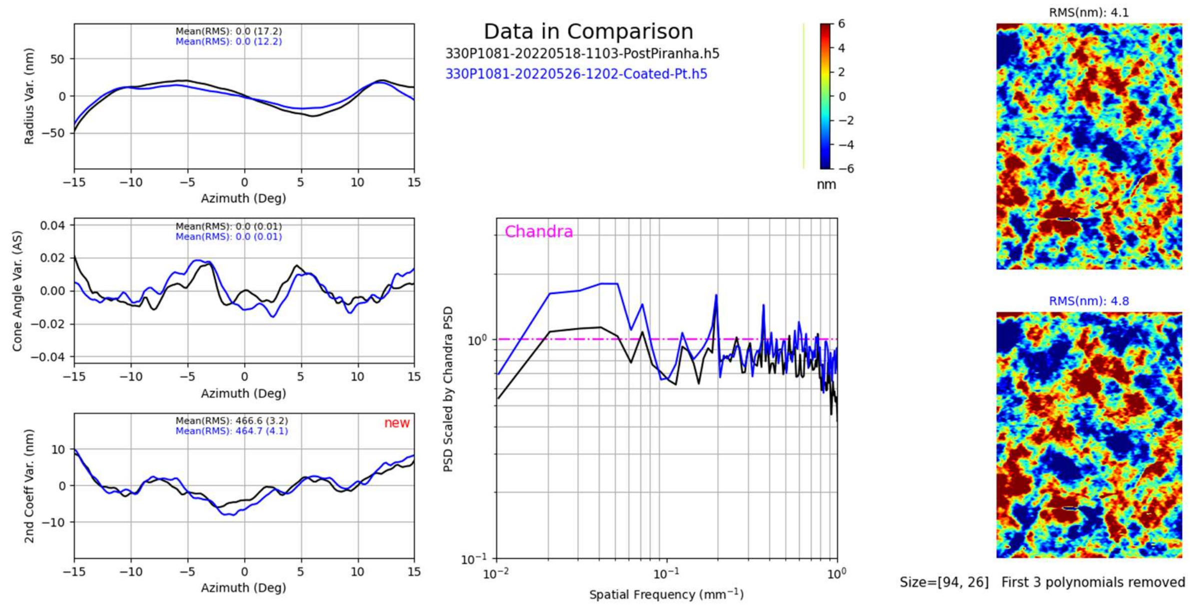

Figure 3-6 Measurement Comparison of 330P1081, 20nm Pt

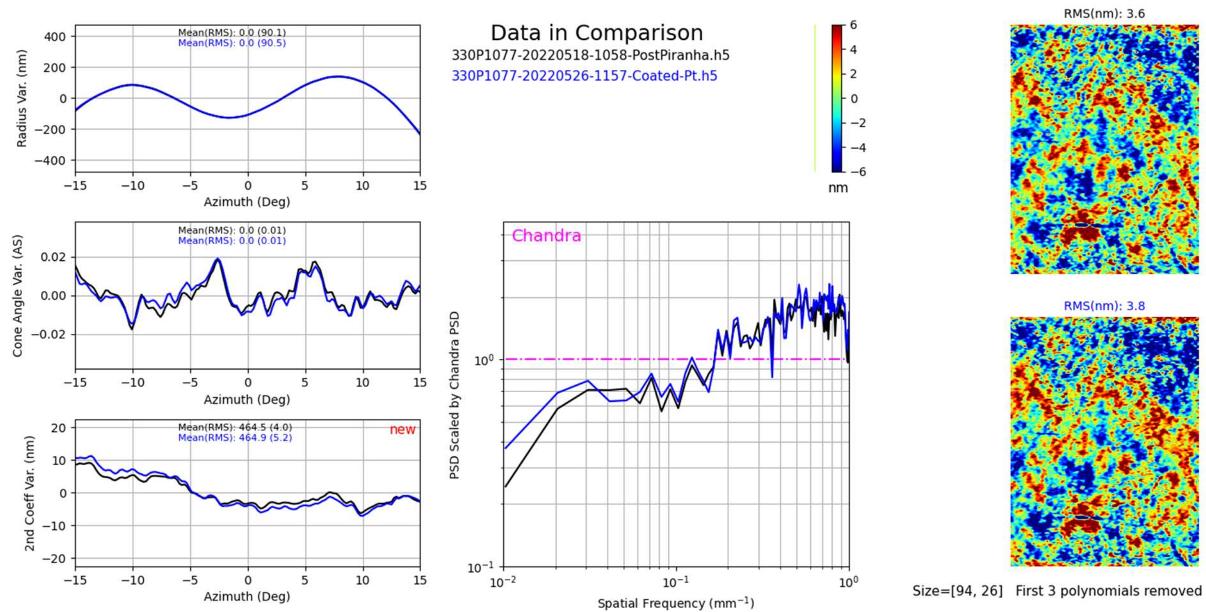

Figure 3-7 Measurement Comparison of 330P1077, 20nm Pt

Downloaded From: https://www.spiedigitallibrary.org/conference-proceedings-of-spie on 01 Sep 2022
Terms of Use: https://www.spiedigitallibrary.org/terms-of-use

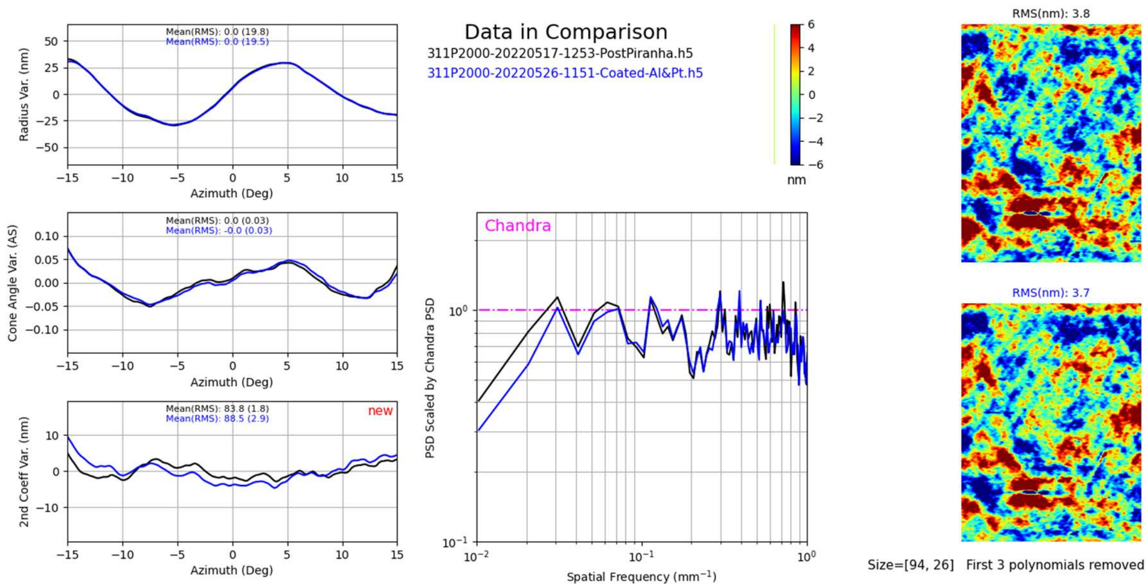

Figure 3-8 Measurement Comparison of 311P2000, 8nm Pt + 7nm Al_2O_3

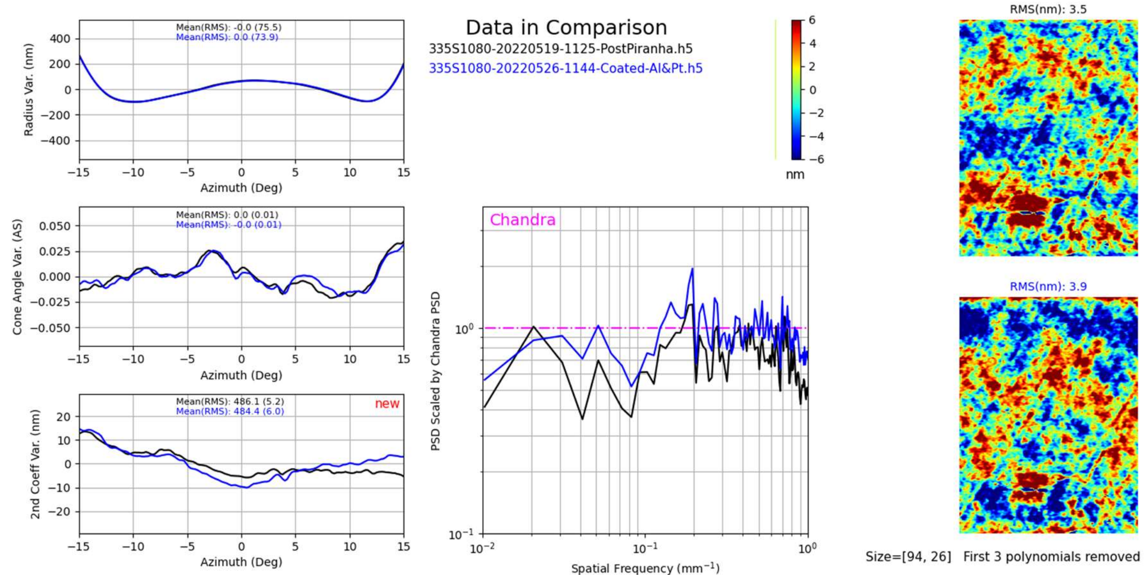

Figure 3-9 Measurement Comparison of 335S1080, 8nm Pt + 7nm Al_2O_3

4. CONCLUSIONS

Two viable methods for coating lightweight silicon optics with high-density materials have been presented. Both methods would provide the required performance at higher energies required for future X-ray telescopes, while still meeting the high-resolution optical performance requirements. Of the two methods, the ALD process is significantly simpler, and therefore more schedule and cost efficient, while also yielding a better resulting figure. The backside compensation technique is shown to be effective when proper care is taken to calibrate the models with measurements and would be suitable if coatings that are not viable with the ALD process are required.

Downloaded From: https://www.spiedigitallibrary.org/conference-proceedings-of-spie on 01 Sep 2022
Terms of Use: https://www.spiedigitallibrary.org/terms-of-use

ACKNOWLEDGEMENTS

- NASA Physics of the Cosmos (PCOS) Program
- NASA ROSES/APRA
- MIT Kavli Institute
- Maryland NanoCenter
- Arradiance

REFERENCES

[1] Tutt, J. H., et al., "The Off-plane Grating Rocket Experiment (OGRE) system overview," SPIE Proc, Vol 10699, p. 106996H, (2018).

[2] Zhang, W. W., et al., "STAR-X: Survey and Time-domain Astrophysical Research eXplorer," SPIE Proc, Vol. 12181-82, these proceedings, (2022).

[3] Gaskin, J. A., et al., "The Lynx X-ray Observatory: concept study overview and status," SPIE Proc, Vol 10699, p. 106990N, (2018).

[4] Zhang, W. W., et al., "Single Crystal Silicon X-ray Optics for Astronomy: high resolution, light weight, and low cost," SPIE Proc, Vol. 12181-36, these proceedings, (2022).

[5] Riveros, R.E., et al., "Fabrication of Lightweight Silicon X-ray Mirrors," SPIE Proc, Vol. 12181-37, these proceedings, (2022).

[6] Chan, K.W., et al., "Mirror alignment and integration for high-resolution astronomical x-ray telescopes," SPIE Proc, Vol. 12181-214, these proceedings, (2022).

[7] Kao, D.B., et al., "Two-Dimensional Thermal Oxidation of Silicon – II. Modeling Stress Effects in Wet Oxides," IEEE Transactions on Electron Devices, Vol. ED-35, No. 1, (1988).

[8] Yao, Y., et al., "Progress of coating stress compensation of silicon mirrors for Lynx x-ray telescope mission concept using thermal oxide patterning method," J. Astron. Telesc. Instrum. Syst 5(2), 021011, (2019).

[9] Chan, K.W., et al., "Coating Thin Mirror Segments for Lightweight X-ray Optics," SPIE Proc, Vol. 8861, p. 88610X, (2013).

[10] Aaltonen, T., et. al., "Atomic Layer Deposition of Iridium Thin Films," Journal of the Electrochemical Society, Vol 151 (8), G489-G492, (2004).

Downloaded From: https://www.spiedigitallibrary.org/conference-proceedings-of-spie on 01 Sep 2022
Terms of Use: https://www.spiedigitallibrary.org/terms-of-use